Surface Faceting Dependence of Thermal Transport in Silicon Nanowires

Frederic Sansoz*

School of Engineering and Materials Science Program, University of Vermont, Burlington, Vermont 05405, United States

S *Supporting Information*

ABSTRACT: Surface faceting on sidewalls is ubiquitously observed during crystal growth of semiconductor nanowires. However, predicting the thermal transport characteristics of faceted nanowires relevant to thermoelectric applications remains challenging. Here, direct molecular dynamics simulations show that thermal conductivity is considerably reduced in crystalline $\langle 111 \rangle$ Si nanowires with periodic sawtooth faceting compared to nanowires of same size with smooth sidewalls. It is discovered that surface phonon scattering is particularly high with $\{100\}$ facets, but less pronounced with $\{113\}$ facets and remarkably low with $\{111\}$ facets, which suggests a new means to optimize phonon dynamics for nanoscale thermoelectric devices. This anomaly is reconciled by showing that the contribution of each facet to surface phonons is due to diffuse scattering rather than to backward scattering. It is further shown that this property is not changed by addition of an amorphous shell to the crystalline core, similar to the structure of experimental nanowires.

KEYWORDS: Thermal conductivity, nanoscale thermoelectrics, surface morphology, sawtooth faceting, semiconductor nanowire
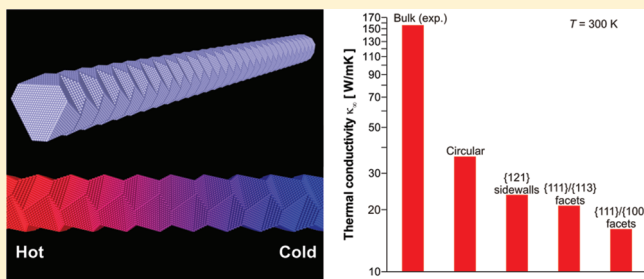
Control over phonon transport is critical to the development of next-generation thermoelectric devices in semiconductors. Thermoelectric efficiency in such devices is usually measured by the figure-of-merit $ZT = S^2 \sigma T / k$ where S is the Seebeck coefficient, σ is the electrical conductivity, κ is the thermal conductivity, and T is the (average) temperature. In crystalline nanowires (NWs), the role of phonon transport becomes increasingly important because spatial confinement in low-dimensional nanostructures is found to considerably reduce κ compared to bulk, while the power factor ($S^2 \sigma$) only deviates slightly.[1-3] Recently, such unique characteristics have been applied to enable high ZT values in Si-based thermoelectric devices incorporating NWs or nanomesh structures.[4-8] Phonon confinement effects in Si NWs result primarily from a dispersion of the phonon spectrum due to surface scattering and therefore depend on the NW diameter and surface structure.[2,9-16] Earlier experiments[5,6] have shown clear evidence for a marked reduction of κ in chemically etched Si NWs with rough surfaces in comparison to smooth NWs of equivalent diameter. Also, previous theoretical reports on Si NWs with either random surfaces[11,13,17,18] or more symmetrical ones consisting of square or triangular steps[18,15] have shown that the surface roughness and the native surface oxide layer behave as secondary scattering phases and act to augment the rates of diffuse reflection and backscattering of phonons at the boundary. Furthermore, Moore et al.[19] have proved theoretically that phonon backscattering due to surface roughness could be extended to NWs presenting periodic sawtooth facets. Unlike random surfaces, surface faceting occurs naturally (and more controllably) on the sidewalls of Si NWs obtained through

metal-catalyzed vapor phase epitaxy. In particular, significant progress has been made experimentally in controlling the surface morphology of $\langle 111 \rangle$-oriented Si NWs with sidewalls varying from atomically smooth $\{121\}$ planes[20,21] to complex sawtooth faceting with either $\{111\}/\{100\}$ facets[22-25] or $\{111\}/\{113\}$ facets.[26-30] Surface faceting at the nanoscale has been found in the past to profoundly influence chemical, mechanical, and electrical properties in crystalline NWs and nanoparticles.[31-36] However, our understanding of the effect of surface faceting on thermal transport in semiconductor NWs is still rather restricted.

In this Letter, using atomistic computer simulations, we examine the impact of NW morphology on thermal conductivity in $\langle 111 \rangle$ Si NWs with particular emphasis on circular, hexagonal, and sawtooth-faceted shapes. A detailed analysis of vibrational density of states (VDOS) between core and surface atoms is carried out for different types of facet to determine the relationship between surface structure and phonon dynamics and to elucidate the surface scattering mechanism controlling thermal transport in these materials. From this study, we show that the macroscopic limit of κ is reduced by 90% in sawtooth-faceted $\{111\}/\{100\}$ Si NWs compared to the experimental bulk conductivity at the same temperature and reduced by 55% compared to NWs of same size with smooth sidewalls. This effect is shown to result from a strong dispersion of surface phonon in $\{100\}$-type facets compared to VDOS of atoms in the core. However,
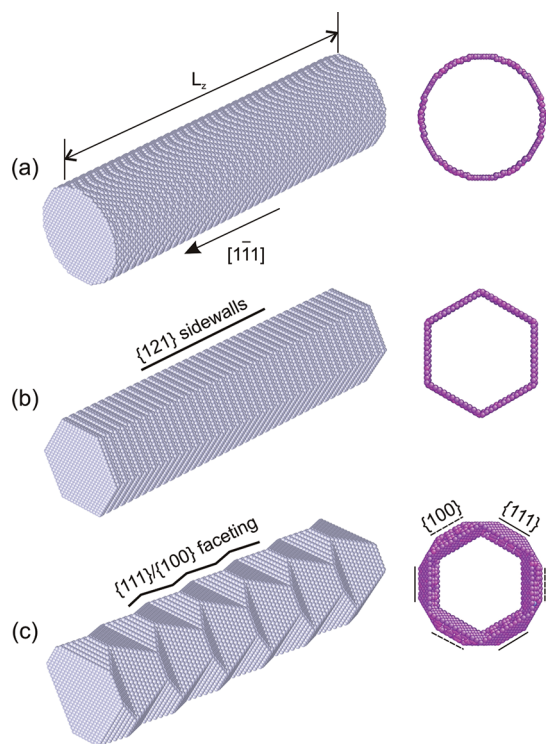
Figure 1. Atomistic models of ⟨111⟩-oriented Si NWs with different surface structures. (a) Cylindrical NW with circular cross section. (b) Cylindrical NW with hexagonal cross section made of flat {121} sidewalls. (c) Sawtooth-faceted NW made of a periodic arrangement of {111}/{100} facets. The lateral dimension is 9.8 nm in all models.

Figure 2. Effects of surface structure on lattice thermal conductivity of ⟨111⟩ Si NWs at 300 K. (a) System size dependence of $1/\kappa$ on $1/L_z$ as predicted by nonequilibrium molecular dynamics simulations. (b) Macroscopic limit of thermal conductivity κ_∞ obtained by extrapolating the lines to $1/L_z \sim 0$, as a function of surface morphology.

the simulations reveal that phonon dispersion is less pronounced with {113}-type facets and absent with {111}-type facets, which suggests that the facet contribution to surface modes is due to diffuse scattering rather than to backward scattering. It is further shown that this property is not altered when adding a shell made of amorphous Si to the crystalline core, which is similar to the surface structure of Si NWs in experiments.

Four types of crystalline, ⟨111⟩-oriented Si NWs with different surface morphologies were studied by using nonequilibrium molecular dynamics (MD) computer simulations (see method description in Supporting Information). The models investigated consisted of smooth, cylindrical surfaces with either circular sidewalls (Figure 1a) or hexagonal, {121}-type sidewalls (Figure 1b), and two types of periodic sawtooth faceting with {111}/{100} facets (Figure 1c) or {111}/{113} facets (not shown). Figure 2a shows the system size-dependence of $1/\kappa$ on $1/L_z$, where L_z is the simulation cell length (Figure 1a), for all structures from our MD computations. It is worth noting that a plot of $1/\kappa$ versus $1/L_z$ is linear due to finite-size effects known to arise in simulation when L_z is smaller than the phonon mean-free path.[37] Figure 2a shows that $1/\kappa$ increases markedly in ⟨111⟩ Si NWs with a diameter of 9.8 nm compared to bulk; however this effect is more pronounced in sawtooth-faceted NWs than smooth ones. This conclusion is consistent with spatial confinement and surface roughness effects on thermal transport described by others. Furthermore, extrapolating each linear trend to $1/L_z \sim 0$ yields the macroscopic limit of thermal conductivity, referred to as κ_∞ in the following (see Supporting Information). Figure 2b shows clearly that κ_∞ is the smallest for sawtooth {111}/{100} NWs with $\kappa_\infty = 16$ W m^{-1} K^{-1}. Such a low conductivity for

crystalline Si corresponds to a reduction in thermal transport of 90% compared to thermal conductivity in bulk Si (111) at 300 K ($\kappa_\infty = 156$ W m^{-1} K^{-1})[38] and up to 55% compared to NWs of same size with circular sidewalls ($\kappa_\infty = 36$ W m^{-1} K^{-1}). For comparison, $\kappa_\infty = 21$ W m^{-1} K^{-1} in sawtooth {111}/{113} NWs, thus suggesting that κ_∞ also depends on the type of surface faceting. It is also worth noting in Figure 2 that κ_∞ is significantly smaller in smooth NWs with flat {121} sidewalls ($\kappa_\infty = 24$ W m^{-1} K^{-1}) than in NWs with a circular cross-section. The fact that this difference is smaller than the variation in cross-sectional area between these two structures (17%) supports the idea that boundary scattering is superior for certain surface orientations than others, as shown below. Using eq (1) in Supporting Information with $\nu = 6500$ m·s^{-1} for the interatomic potential used in this study,[37,39] we also find that the phonon mean free path decreases from 69.6 nm from bulk to 7.2 nm in {111}/{100} NWs, which therefore suggests that the contribution of surface phonons is strong in the latter case.

Moreover, Figure S1 (see Supporting Information) tends to indicate that κ_∞ decreases quasi-linearly as the faceting height and length increase in sawtooth-faceted NWs. Such a linear scaling of κ with facet height differs markedly from past theoretical
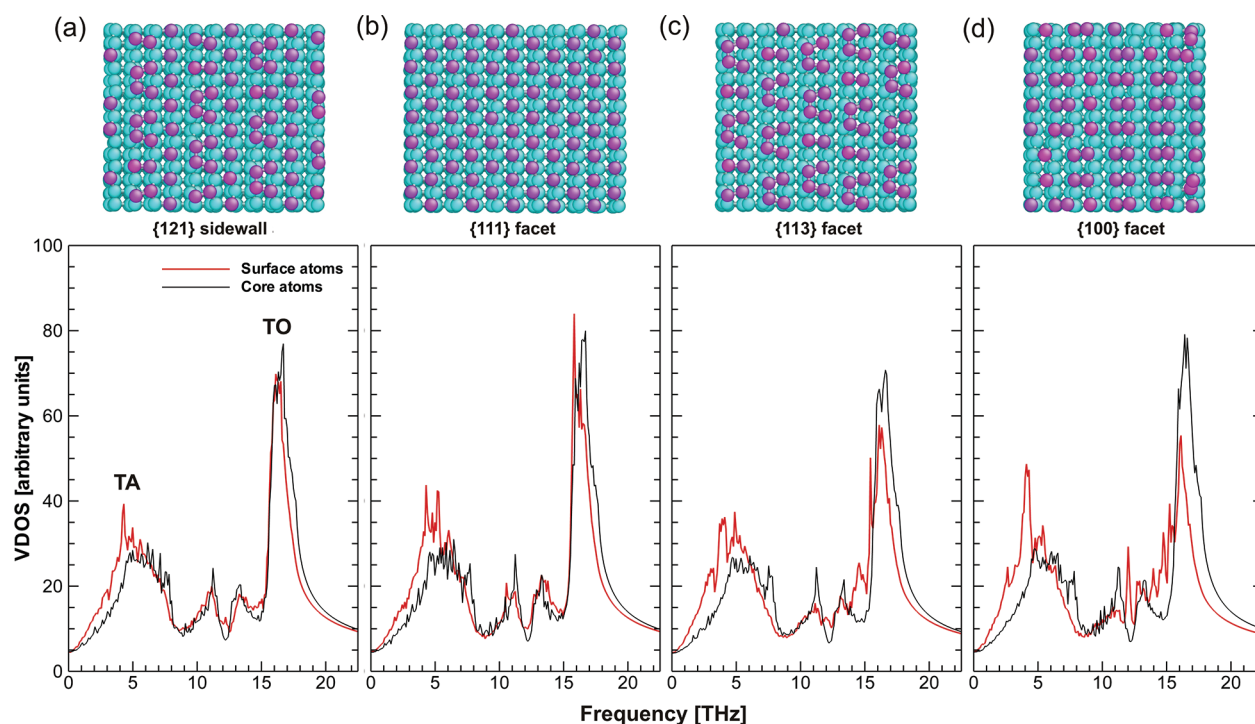
Figure 3. Average VDOS analysis of atoms located in the core or at the surface of simulated Si NWs for different types of surface facets: (a) {121} sidewall, (b) {111} facet, (c) {113} facet, and (d) {100} facet. The frequency domains for both transverse acoustic (TA) and optical (TO) modes are also indicated in (a).

predictions by Martin et al.[13] in rough Si NWs. In particular, these authors have obtained that considering random peaks at the Si−SiO$_2$ interface to serve as constrictions to phonon propagation would lead to a quadratic dependence of κ on the root-mean-square roughness height. This discrepancy therefore implies that the surface scattering mechanism is different in the present study. A linear relationship could also indicate that thermal transport is subjected to partially backward scattering by the sawtooth morphology.[19] This hypothesis is further investigated in what follows.

Atomistic simulations and ab initio calculations have been used extensively to study vibrational properties because κ is strongly influenced by changes in VDOS. Past simulation studies in a variety of Si nanostructures ranging from pure crystalline Si nanoparticles[40] and NWs[41,10] to core−shell Si NWs with amorphous or crystalline layers[42,11,17,43] have shown clear changes from the bulk VDOS, because the contribution of surface modes to the total VDOS becomes more important for smaller NWs due to the increasing fraction of atoms located at the surface relative to the fraction of atoms in the core. The primary changes are twofold: (1) an increase of the VDOS at low frequencies, which is amplified by the fact that the phonon spectrum near the transverse-acoustic (TA) mode becomes more linear with decreasing size,[40] and (2) a pronounced transfer of weight from the high-frequency transverse-optical (TO) peak to intermediate frequencies.[11] Here, using Figure 3 we studied the changes in average VDOS predicted between atoms in the core and those from different types of surface facets (see method description in Supporting Information). In all cases, the behavior of the core atoms was found similar to the bulk-like modes.[40] Also, the VDOS of flat {121} sidewalls (Figure 3a) was found to coincide with that of core atoms for most phonon modes except for the
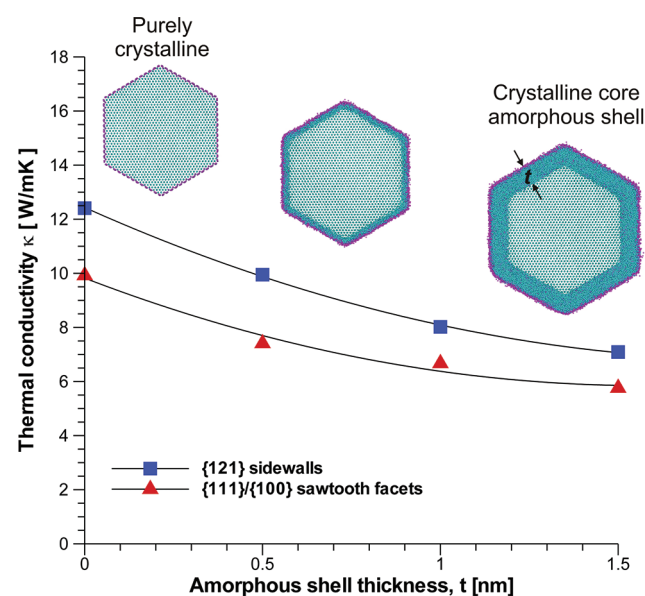
low-frequency TA mode where a slight increase in VDOS could be detected due to the localization of phonons at the free surface. On the contrary, significant changes in VDOS were observed with atoms on {100} facets compared to core atoms as shown in Figure 3d. These changes were characterized by a shift to lower frequencies and an increase in height of the TA peak in the range 0−5 THz, as well as by a significant dispersion to intermediate frequencies and a decrease in height of the TO peak in the range 12−20 THz. The changes associated with the VDOS of atoms on {113} facets were also found significant, as shown in Figure 3c, but relatively less than for atoms on {100} facets. This agrees well with the predictions presented in Figure 2b where κ_∞ was found smaller with sawtooth {111}/{113} faceting than sawtooth {111}/{100} faceting. Remarkably, however, it can be observed in Figure 3b that the VDOS of atoms on {111} facets in sawtooth NWs shows no significant phonon dispersion compared to VDOS in core atoms and is somewhat similar to that of atoms on {121} facets in smooth NWs presented in Figure 3a.

Since κ is strongly affected by dispersion of surface phonons at each frequency, the above result enables us to conclude that {100}-type facets and, to a lesser extent, {113}-type facets contribute more significantly to the overall reduction of κ than {111}-type facets and {121}-type facets. An attempt is made in the following to understand the physical origin of this phenomenon. It is acknowledged that when a lattice wave strikes the surface of a facet, the reflected wave is subjected to both specular and diffuse scattering from the microscopic surface roughness and to backscattering emanating from the sawtooth structure bouncing back phonons. Surprisingly, the absence of surface phonon dispersion in {111} facets is in stark contrast with the stronger dispersion predicted in {113} facets. It is emphasized in Table 1 that the angle made by {111} facets with the NW axis is

Table 1. Surface Facet Orientation with Respect to NW Axis and ⟨100⟩ Crystallographic Directions

type of surface facet	angle with ⟨111⟩ NW axis (deg)	maximum angle with ⟨100⟩ directions (deg)
{100}	35	90
{111}	19	35
{113}	10	65
{121}	0	55

Figure 4. Thermal conductivity for hexagonal and sawtooth-faceted Si NWs consisting of a crystalline core and an amorphous shell, as a function of amorphous shell thickness. L_z = 82 nm in all models.

almost twice that in {113} facets. Accordingly, it could be predicted that phonon backscattering effects should be more important with the former than the latter,[19] which contradicts the results presented in Figure 3. This clearly suggests that the facet contribution to surface modes is more likely related to diffuse scattering than to backward scattering.

Furthermore, an analysis of possible scattering mechanisms on free surfaces can be made by invoking two hypotheses. First, Figure 3 shows a close-up view on the atomic structure of each facet type after thermal relaxation revealing that {100} and {113} surface facets have 2 × 1 dimer reconstructions and 3 × 1 surface reconstructions,[44] respectively, which is common for Si. Such reconstructed surface structures differ in complexity from more regular, stable structures observed on {111} surface facets. This is in good agreement with past experimental measurements in low-dimensional Si systems showing that the surface energy at equilibrium is larger by 10−15% on {100} and {113} facets than on {111} facets.[45] Therefore, one could possibly conclude that TO modes are more likely dispersed on high-energy boundaries, such as {100} and {113} facets due to surface imperfections (for example, the presence of steps and dangling bonds). In the present work, however, this argument breaks down because {112} facets and {113} facets, whose surface reconstructions are found to be very close in Figure 3, exhibit marked difference in VDOS at the free surface. Second, a recent theoretical study by Aksamija and Knezevic[46] has also

demonstrated that diffuse boundary scattering is always stronger on Si (100) surfaces than Si (111) surfaces because TA phonon velocities in crystalline Si are mostly directed along ⟨100⟩ directions. As such TA modes are found to scatter very strongly from boundaries oriented parallel to (100) because these surfaces are perpendicular to the lattice wave propagation. Similarly, Table 1 shows that in the present study the ⟨100⟩ directions make the highest angle with {100} and {113} facets and the lowest one with {111} facets, which is more in line with the VDOS predictions presented in Figure 3. Surprisingly, based on the same analysis, this table also demonstrates that diffuse scattering should be less favorable on sawtooth {111} facets than on flat {121} sidewalls.

In order to confirm that the dependence of thermal transport on surface facets in Si NWs is controlled by anisotropic effects on phonon propagation, we computed thermal conductivities for Si NWs with a crystalline core of same size and morphology (either hexagonal or sawtooth {111}/{100} faceted) and an amorphous shell of varying thickness (see description of methods in Supporting Information). The results presented in Figure 4 demonstrate that, while the amorphous shell contributes to a significant reduction in κ as the shell thickness increases, the overall difference between different types of morphology remains unchanged. The atomic structure of the interface between the crystalline core and the amorphous shell is arguably different from that of free surfaces in pure crystalline Si NWs; however Figure 4 shows that κ is always larger in NWs with {121} sidewalls than in NWs with {111}/{100} faceting regardless of the amorphous shell thickness. This key finding emphasizes that the present theoretical study is relevant to understanding thermal transport in faceted Si NWs in experiments, because realistic surfaces are most often associated with the presence of amorphous native oxides in Si.

In summary, using nonequilibrium atomistic simulations the present study has shown that thermal conductivity is reduced considerably at 300 K in sawtooth Si NWs with either {111}/{100} faceting or {111}/{113} faceting, compared to smooth Si NWs of equivalent diameter, even with the addition of an amorphous shell to the crystalline core. We demonstrate that the macroscopic limit of κ decreases to 16 W m^{-1} K^{-1} in crystalline Si NWs with periodic sawtooth {111}/{100} facets. This value represents a significant reduction of up to 90% compared to bulk and more than 55% compared to smooth NWs with flat {121} sidewalls. An analysis of VDOS between core and surface atoms also revealed that the loss in thermal transport coincides with a strong dispersion of the TA and TO phonons peaks on {100} facets. A major conclusion is that this characteristic appears to be less pronounced with {113} facets and almost absent with {111} facets. This anomaly was reconciled by showing that the contribution of each facet to surface modes is due to diffuse scattering rather than to backscattering. These conclusions therefore provide a new approach to control phonon dynamics in nanoscale Si-based thermoelectric devices, and are relevant to other semiconductor NW systems where surface faceting phenomena are prominent.

■ ASSOCIATED CONTENT

⑤ Supporting Information. 1. Description of Computational Methods. 2. Supporting Figures. 3. Supporting References. This material is available free of charge via the Internet at http://pubs.acs.org.

■ AUTHOR INFORMATION

Corresponding Author
*E-mail: frederic.sansoz@uvm.edu.

■ REFERENCES

(1) Hicks, L. D.; Dresselhaus, M. S. *Phys. Rev. B* **1993**, *47* (24), 16631–16634.

(2) Li, D. Y.; Wu, Y. Y.; Kim, P.; Shi, L.; Yang, P. D.; Majumdar, A. *Appl. Phys. Lett.* **2003**, *83* (14), 2934–2936.

(3) Chen, X.; Wang, Y. C.; Ma, Y. M.; Cui, T.; Zou, G. T. *J. Phys. Chem. C* **2009**, *113* (31), 14001–14005.

(4) Boukai, A. I.; Bunimovich, Y.; Tahir-Kheli, J.; Yu, J. K.; Goddard, W. A.; Heath, J. R. *Nature* **2008**, *451* (7175), 168–171.

(5) Hochbaum, A. I.; Chen, R. K.; Delgado, R. D.; Liang, W. J.; Garnett, E. C.; Najarian, M.; Majumdar, A.; Yang, P. D. *Nature* **2008**, *451* (7175), 163–U5.

(6) Hippalgaonkar, K.; Huang, B.; Chen, R.; Sawyer, K.; Ercius, P.; Majumdar, A. *Nano Lett.* **2010**, *10* (11), 4341–4348.

(7) Tang, J.; Wang, H.-T.; Lee, D. H.; Fardy, M.; Huo, Z.; Russell, T. P.; Yang, P. *Nano Lett.* **2010**, *10* (10), 4279–4283.

(8) Yu, J. K.; Mitrovic, S.; Tham, D.; Varghese, J.; Heath, J. R. *Nat. Nanotechnol.* **2010**, *5* (10), 718–721.

(9) Lacroix, D.; Joulain, K.; Damian Terris, D.; Lemonnier, D. *Appl. Phys. Lett.* **2006**, *89*, 103104.

(10) Ponomareva, I.; Srivastava, D.; Menon, M. *Nano Lett.* **2007**, *7* (5), 1155–1159.

(11) Donadio, D.; Galli, G. *Phys. Rev. Lett.* **2009**, *102* (19), 195901.

(12) Markussen, T.; Jauho, A. P.; Brandbyge, M. *Phys. Rev. Lett.* **2009**, *103* (5), 055502.

(13) Martin, P.; Aksamija, Z.; Pop, E.; Ravaioli, U. *Phys. Rev. Lett.* **2009**, *102* (12), 125503.

(14) Shi, L. H.; Yao, D. L.; Zhang, G.; Li, B. W. *Appl. Phys. Lett.* **2009**, *95* (6), 063102.

(15) Doerk, G. S.; Carraro, C.; Maboudian, R. *ACS Nano* **2010**, *4* (8), 4908–4914.

(16) Liu, L.; Chen, X. *J. Appl. Phys.* **2010**, *107* (3), 033501.

(17) Donadio, D.; Galli, G. *Nano Lett.* **2010**, *10* (3), 847–851.

(18) Kazan, M.; Guisbiers, G.; Pereira, S.; Correia, M. R.; Masri, P.; Bruyant, A.; Volz, S.; Royer, P. *J. Appl. Phys.* **2010**, *107*, 083503.

(19) Moore, A. L.; Saha, S. K.; Prasher, R. S.; Shi, L. *Appl. Phys. Lett.* **2008**, *93* (8), 083112.

(20) Arbiol, J.; Morral, A. F. I.; Estrade, S.; Peiro, F.; Kalache, B.; Cabarrocas, P. R. I.; Morante, J. R. *J. Appl. Phys.* **2008**, *104* (6), 064312.

(21) Moutanabbir, O.; Senz, S.; Scholz, R.; Alexe, M.; Kim, Y.; Pippel, E.; Wang, Y.; Wiethoff, C.; Nabbefeld, T.; Meyer zu Heringdorf, F.; Horn-von Hoegen, M. *ACS Nano* **2011**, *5* (2), 1313–1320.

(22) Ross, F. M.; Tersoff, J.; Reuter, M. C. *Phys. Rev. Lett.* **2005**, *95* (14), 146104.

(23) Li, F.; Nellist, P. D.; Cockayne, D. J. H. *Appl. Phys. Lett.* **2009**, *94* (26), 263111.

(24) Li, F.; Nellist, P. D.; Lang, C.; Cockayne, D. J. H. *ACS Nano* **2010**, *4* (2), 632–636.

(25) Oehler, F.; Gentile, P.; Baron, T.; Ferret, P.; Den Hertog, M.; Rouviere, J. *Nano Lett.* **2010**, *10* (7), 2335–2341.

(26) David, T.; Buttard, D.; Schülli, T.; Dallhuin, F.; Gentile, P. *Surf. Sci.* **2008**, *602* (15), 2675–2680.

(27) Wiethoff, C.; Ross, F. M.; Copel, M.; Horn-von Hoegen, M.; Meyer zu Heringdorf, F.-J. *Nano Lett.* **2008**, *8* (9), 3065–3068.

(28) Sivakov, V. A.; Scholz, R.; Syrowatka, F.; Falk, F.; Gosele, U.; Christiansen, S. H. *Nanotechnology* **2009**, *20*, 405607.

(29) Doerk, G. S.; Radmilovic, V.; Maboudian, R. *Appl. Phys. Lett.* **2010**, *96*, 123117.

(30) Xu, T.; Nys, J. P.; Addad, A.; Lebedev, O. I.; Urbieta, A.; Salhi, B.; Berthe, M.; Grandidier, B.; Stievenard, D. *Phys. Rev. B* **2010**, *81* (11), 115403.

(31) Zhao, Y.; Yakobson, B. I. *Phys. Rev. Lett.* **2003**, *91* (3), 035501.

(32) Leach, A. M.; McDowell, M.; Gall, K. *Adv. Funct. Mater.* **2007**, *17* (1), 43–53.

(33) Barnard, A. S. *Cryst. Growth Des.* **2009**, *9* (11), 4860–4863.

(34) Barnard, A. S.; Young, N. P.; Kirkland, A. I.; van Huis, M. A.; Xu, H. *ACS Nano* **2009**, *3* (6), 1431–1436.

(35) Deng, C.; Sansoz, F. *ACS Nano* **2009**, *3* (10), 3001–3008.

(36) Deng, C.; Sansoz, F. *Phys. Rev. B* **2010**, *81* (15), 155430.

(37) Schelling, P. K.; Phillpot, S. R.; Keblinski, P. *Phys. Rev. B* **2002**, *65* (14), 144306.

(38) Glassbrenner, C. J.; Slack, G. A. *Phys. Rev. B* **1964**, *134*, A1058–A1069.

(39) Muñoz, E.; Lu, J.; Yakobson, B. I. *Nano Lett.* **2010**, *10* (5), 1652–1656.

(40) Meyer, R.; Comtesse, D. *Phys. Rev. B* **2011**, *83* (1), 014301.

(41) Becker, B.; Schelling, P. K.; Phillpot, S. R. *J. Appl. Phys.* **2006**, *99* (12), 123715.

(42) Mingo, N.; Yang, L. *Phys. Rev. B* **2003**, *68* (24), 245406.

(43) Hu, M.; Giapis, K. P.; Goicochea, J. V.; Zhang, X.; Poulikakos, D. *Nano Lett.* **2011**, *11* (2), 618–623.

(44) Yu, L. *Appl. Phys. Lett.* **2010**, *97* (2), 023107.

(45) Eaglesham, D. J.; White, A. E.; Feldman, L. C.; Moryia, M.; Jacobson, D. C. *Phys. Rev. Lett.* **1993**, *70* (11), 1643–1647.

(46) Aksamija, Z.; Knezevic, I. *Phys. Rev. B* **2010**, *82* (4), 045319.